Available online at www.sciencedirect.com

ScienceDirect

www.elsevier.com/locate/jmbbm

CrossMark

Research Paper

Strain-induced microstructural rearrangement in ultra-high molecular weight polyethylene for hip joints: A comparison between conventional and vitamin E-infused highly-crosslinked liners

Yasuhito Takahashi^a, Kengo Yamamoto^a, Takaaki Shishido^a,
Toshinori Masaoka^a, Toshiyuki Tateiwa^a, Leonardo Puppulin^b,
Giuseppe Pezzotti^{b,*}

^aDepartment of Orthopaedic Surgery, Tokyo Medical University, 6-7-1, Nishishinjuku, Shinjuku-ku, 160-0023 Tokyo, Japan

^bCeramic Physics Laboratory and Research Institute for Nanoscience, Kyoto Institute of Technology, Sakyo-ku, Matsugasaki, 606-8585 Kyoto, Japan

ARTICLE INFO

Article history:

Received 5 June 2012

Accepted 20 December 2012

Available online 11 January 2013

Keywords:

Vitamin E

UHMWPE

Microstructure

Strain

Raman spectroscopy

ABSTRACT

Infusion of vitamin E (α -tocopherol) in highly crosslinked ultra-high molecular weight polyethylene (UHMWPE) liners has been conceived to achieve superior oxidation stability while preserving enhanced mechanical properties as compared to post-irradiation remelted liners. However, the presence of an antioxidant in the material microstructure brings an issue of concern in whether a “foreign substance” might reduce radiation crosslinking efficiency and/or change microstructural characteristics by diffusing into UHMWPE. The key to clarify this fundamental issue resides in performing a quantitative evaluation of the obtained material structure and its polymeric chain mobility on the molecular scale. In this paper, a Raman spectroscopic examination is presented of molecular orientation and phase fractions in as-processed vitamin E-infused UHMWPE acetabular liners in comparison with a model (undoped and unirradiated/uncrosslinked) and a conventional (undoped and 33 kGy-sterilized by gamma-irradiation) UHMWPE liners. The microstructural responses of structurally different liners to externally applied compressive strain were also monitored. The main results of the spectroscopic analyses can be summarized as follows: (i) preliminary gamma irradiation reduced the fraction of amorphous phase and increased the degree of molecular alignment, the vitamin E-infused liner preserving the crystallinity level achieved by the 100-kGy irradiation injected before infusion; (ii) the presence of vitamin E significantly promoted orientational randomness, which increased with increasing compressive strain magnitude, a phenomenon beneficial to minimize strain-softening-assisted wear phenomena.

© 2012 Elsevier Ltd. All rights reserved.

*Corresponding author. Tel./fax: +81 75 724 7568.

E-mail address: pezzotti@kit.ac.jp (G. Pezzotti).

1. Introduction

In the last 15 years, crosslinked polyethylene has been introduced in the orthopedic market to counteract the formation *in vivo* of polyethylene wear debris, responsible for a cascade of biological reactions ultimately leading to osteolysis and to the need of revision surgery (Amstutz et al., 1992; Digas et al., 2004). According to available statistics, this detrimental effect yet represents the most critical issue in hip arthroplasty and it was found to be the most limiting factor in the longevity of artificial hip implants (Harris, 1995). Crosslinking polyethylene molecular chains, which can be promoted upon exposure to high-energy irradiations (e.g., gamma rays), can greatly increase wear resistance, thus reducing debris formation and, with it, the probability for osteolysis to occur. The main shortcoming of this procedure is that crosslinking also unavoidably involves the formation of free radicals, which remain trapped in a chemically unstable equilibrium within the material microstructure after irradiation (Oral and Muratoglu, 2007). If left unstabilized, free radicals could be highly reactive to oxygen, which eventually starts a chain reaction ultimately causing oxidative degradation over time. Following the above notions, modern UHMWPE hip components can be classified according to the specific method used by manufacturers to counteract oxidation degradation processes in presence of residual free radicals. Some manufacturers proposed to reduce the free-radical concentration by re-heating above the melting temperature (i.e., remelting) the material after crosslinking. Remelting would allow substantial recombination of free radicals and thus reduces free-radical concentration below detectable levels, which in turn increases oxidation resistance. However, remelting can be detrimental to the structural properties of polyethylene, which manifests with a drop down in tensile strength and fatigue resistance (Baker et al., 2003; Bradford et al., 2004; Gencur et al., 2003). As an alternative processing procedure, annealing of the polyethylene structure below its melting temperature (i.e., after crosslinking) was also found to produce annihilation of free radicals while also allowing for the detainment of strength and fatigue resistance properties. However, with simply annealing the polyethylene liner, there is no guaranty that all the free radicals trapped at the microstructural scale could re-combine and, therefore, a residual fraction of free radicals eventually remains in the liner, which oxidizes *in vivo* (Currier et al., 2007; Muratoglu et al., 2003; Wannomae et al., 2006). An optimized multiple-step (sequential) annealing process without terminal gamma sterilization has been recently proposed and shown to greatly increase oxidative stability above the previous generation of conventionally annealed polyethylenes (Wang et al., 2006; Collier et al., 2003). As an alternative procedure to sequential annealing, polyethylene liners have been processed below the melting temperature in order to maintain unchanged the structural characteristics of irradiated samples but, concurrently, vitamin E has also been infused in their microstructure (Oral et al., 2006, 2007; Oral and Muratoglu, 2011). Vitamin E is a collective term for the group of tocopherols, of which α -tocopherol shows the best properties as an antioxidant, namely a substance that

stabilizes free radicals and prevents oxidative degradation (Lerf et al., 2010; Oral et al., 2006; Oral and Muratoglu, 2011). According to the above reason, sequential annealing and E-vitamin infusion are nowadays the two most advanced processing options that can be offered by manufacturers for elongating the lifetime of irradiated UHMWPE liners. In other words, these two options represent the cutting edge technological developments in microstructural design of biomedical polyethylene.

In this paper, we build upon the reported notion of anti-oxidative effects by vitamin E-infused polyethylene liners and further inquire about the structure of this newly developed material at the molecular scale. Infusing vitamin E into irradiated polyethylene is claimed to annihilate free radicals in the polyethylene by donating a hydrogen atom from the OH⁻ group of its ring structure and thus transferring the free radicals from the polyethylene chain to the vitamin E molecule (Bracco et al., 2007; Burton and Ingold, 1981; Kamal-Eldin and Appelqvist, 1996; Lerf et al., 2010; Oral et al., 2006; Oral and Muratoglu, 2011). However, while the “chemical” rationale supporting the anti-oxidative capacity of vitamin E-infused (or blended) liners is clearly stated in the published literature, the material remains almost completely unexplored with respect to its actual three-dimensional structure on the molecular scale. Moreover, its microstructural response to externally applied (compressive) load, which quantitatively reflects the degree of mobility of its molecular assembly, is yet conspicuously unknown. We shall attempt here to provide those missing notions and show spectroscopic characterizations of the newly launched vitamin E-infused liners in comparison to a model (i.e., commercially unavailable) polyethylene liner made from the same resin (undoped and non-irradiated) and undoped UHMWPE liners subjected to the same gamma-sterilization procedure (i.e., with a dose of 33-kGy) as the vitamin E-infused liners. These undoped liners represent the previous generation UHMWPE acetabular components commercialized by the same maker. The spectroscopic comparison will clarify the effect of the vitamin E dopant on the developed material microstructure and on its deformation response to external load.

2. Materials and methods

Three types of acetabular liners were analyzed, which had gone through a different manufacturing process. All liners had a diameter of 32 mm and were provided by Biomet Inc., Warsaw, IN, USA. One type of liner was the newly launched liner E1[®], available on the international market since 2007. Another type of component belonged to a former generation of polyethylene, the brand ArCom[®], which was clinically introduced in 1995 and it is currently commercially available. For comparison, we also examined a model liner, which underwent no irradiation, no anti-oxidative stabilization, and no sterilization. The model liner, the brands ArCom[®] and E1[®] will be henceforth referred to as Liner A, B, and C, respectively. Manufacturing of all three types of liner commonly started from isostatically compression molded GUR 1050 resins. In the case of Liner B, no gamma irradiation and no anti-oxidative stabilization were made, but terminal

released and the sample allowed fully recovering the anelastic strain component for additional 24 h, so that only plastic strain remained stored in the studied microstructure. Compression tests were systematically performed on five samples for each type of investigated material and the compressive load, stepwisely applied, was set to achieve predetermined levels of plastic strains. The residual (plastic) strain was measured along the sample long axis by means of a micrometer caliper, and the deformed samples analyzed by Raman spectroscopy. Spectroscopic characterizations revealed the modifications induced by compressive strain on the original microstructure of the acetabular components, phenomenologically reproducing the conditions encountered during *in vivo* loading.

All Raman spectra were collected at room temperature with a triple monochromator spectrometer (T-64000, Horiba/Jobin-Yvon, Kyoto, Japan) equipped with a high-resolution CCD camera. A spectral resolution of 0.40 cm^{-1} was achieved by means of an 1800 l/mm grating. The excitation source was a 488.0 nm Ar-ion laser (Stabilite 2017-Spectra Physics, Mountain View, CA) yielding a power of approximately 35 mW on the UHMWPE liner surface. Spectral integration times were typically 5 and 10 s for unpolarized and polarized spectra, respectively. Each recorded spectrum was averaged over three successive measurements at each selected location.

The confocal configuration of the probe adopted throughout the present experiment corresponded to a $\times 100$ objective; numerical aperture (N.A.), focal length, and pinhole diameter were fixed as 0.7 , 6.0 mm , and $100\text{ }\mu\text{m}$, respectively. The focal plane of the confocal probe was gradually shifted down to several hundreds of micron below the sample surface to non-destructively obtain spectral profiles toward the central region of the sample, as shown in detail in a previous work (Pezzotti et al., 2007). Spectral deconvolution of all the recorded spectra into sub-bands was achieved according to an automatic fitting algorithm with computational software (Labspec 3, Horiba/Jobin-Yvon, Kyoto, Japan). Mixed Gaussian/Lorentzian curves were used throughout the spectral fitting computations. For each type of studied polyethylene, the results of confocal Raman assessments were averaged on five different samples compressively loaded in order to achieve the same deformation displacements.

Mathematical data treatment, according to the theory described in the following section, was performed with the aid of commercially available software (Mathematica 7; Wolfram Research Inc., IL, USA).

3. Theory and calculation

3.1. Computations of amorphous and crystalline phase fractions

In the case of volume fractional assessments of amorphous (α_a) and crystalline (α_c) phases, we used the intensity of vibrational bands located at 1080 , 1296 , 1310 , and 1418 cm^{-1} , as obtained from unpolarized Raman spectra. The two broad bands at 1080 and 1310 cm^{-1} , which are assigned to the amorphous (matrix)

phase of the polymer, result from C–C stretching and twisting vibrational modes, respectively. On the other hand, the bands at 1296 and 1418 cm^{-1} , which arise from the crystalline phase, possess CH_2 twisting and bending modes, respectively. The relative integrated intensity of the peak located at 1080 and 1418 cm^{-1} can be used to approximate the volume fractions of amorphous and crystalline phase, respectively (Glotin and Mandelkern, 1982; Rull et al., 1978; Strobl and Hagedorn, 1978). Computations of phase fractions were made according to the following equations (Glotin and Mandelkern, 1982; Rull et al., 1993; Strobl and Hagedorn, 1978):

$$\alpha_a = \frac{I_{1080}}{0.79(I_{1296} + I_{1310})} \quad (1)$$

$$\alpha_c = \frac{I_{1418}}{0.46(I_{1296} + I_{1310})} \quad (2)$$

where I is the integrated intensity of the Raman band whose wavenumber is identified by the subscript. Note also that the sum ($\alpha_a + \alpha_c$) might locally be <1 , because of the possible presence of a minor fraction of matter in an anisotropic intermediate disordered state (i.e., usually referred to as the “third phase” (Naylor et al., 1995)). Locations at which ($\alpha_a + \alpha_c$) results slightly >1 instead reflect the experimental error involved with fractional measurements by Raman spectroscopy (in the order of $<0.5\%$).

Microstructural modifications induced by uniaxial plastic strain were monitored as a function of depth below the concave surface of each sample. At each depth, an automated sample stage with sub-micrometric step precision was employed to collect square maps. The typical map size was $500 \times 500\text{ }\mu\text{m}^2$ with a square mesh of $25\text{ }\mu\text{m}$ steps (for a total of $21 \times 21 = 441$ measurement points per each map). Therefore, for each step of deformation and type of polyethylene, the acquired spectrum represented an average over 1323 spectra.

3.2. Computations of molecular orientation patterns

Assessments of preferential molecular orientation were performed by analyzing the spectroscopic behavior of the Raman band located at 1130 cm^{-1} , which is related to the C–C stretching vibration ($A_g + B_{1g}$ mode). The dependence of Raman intensity on crystallographic orientation in parallel polarization was theoretically modeled with respect to its dependences on three Euler angles in space, according to the following equation (Takahashi et al., 2010):

$$I_{A_g+B_{1g}}^{\parallel} = A \left\{ \alpha [c \sin^2 \theta \sin^2 \chi + a (\sin \varphi \cos \chi + \cos \theta \cos \varphi \sin \chi)^2 + b (\cos \varphi \cos \chi - \cos \theta \sin \varphi \sin \chi)^2]^2 + (1-\alpha) [-2d (\sin \varphi \cos \chi + \cos \theta \cos \varphi \sin \chi) (\cos \varphi \cos \chi - \cos \theta \sin \varphi \sin \chi)]^2 \right\} + \Gamma \quad (3)$$

In Eq. (3), A and Γ represent numerical constants that depend on the instrumental configuration and on the spectral band employed; α is a fitting parameter that takes into account the contribution of A_g mode to the observed Raman band and it is also related to the orientation of the molecular chains. The Raman tensor parameters for A_g and B_{1g} modes, which pertain to the 1130 cm^{-1} Raman band and compare as multiplicative factors in Eq. (3) ($a=0.260$, $b=0.202$, $c=-0.898$

and $d = -0.664$), have been determined in previous papers (Takahashi et al., 2010). Eq. (3) was employed to measure at each individual Euler angle indicating the average orientation directions of the molecular chains, while the statistical distribution around such orientation axis was evaluated by means of the so-called orientation distribution function (ODF), $f(\beta)$. The ODF was obtained from Raman spectra collected in confocal/polarized configuration were at different azimuthal angles, χ , using a rotating jig placed under the microprobe. In Fig. 2(b), a schematic draft is shown that explains the experimental set-up adopted for in-plane rotation assessments and our choice of Euler angles. In this particular case, Raman spectra were collected using sheet polarizers in parallel configuration with respect to the incident laser polarization vector. Particular care was taken in order to align the axis of the microscope with the axis of the rotation jig. At each investigated location, polarized Raman spectra were collected at 19 different azimuthal angles within the interval $0^\circ \leq \chi \leq 180^\circ$, with sequential steps of 10° . Each data point in the plots of azimuthal angular dependencies shown in the remainder of this paper was calculated from a value averaged over twenty rotations performed at different locations of each deformed prismatic sample for each investigated strain value. From the computational side, a working equation that includes both Raman selection rules and molecular distribution patterns was then set, as follows (Takahashi et al., 2010):

$$I_{\text{exp}}^{\parallel}(\theta, \varphi, \chi) = \frac{\int_{\gamma=0}^{\gamma=2\pi} \int_{\alpha=0}^{\alpha=2\pi} \int_{\beta=0}^{\beta=2\pi} I_{A_g+B_{1g}}^{\parallel}(\theta, \varphi, \chi) f(\beta) \sin \beta d\beta d\alpha d\gamma}{\int_{\gamma=0}^{\gamma=2\pi} \int_{\alpha=0}^{\alpha=2\pi} \int_{\beta=0}^{\beta=2\pi} f(\beta) \sin \beta d\beta d\alpha d\gamma} \quad (4)$$

with the polarized Raman intensity, $I_{\text{exp}}^{\parallel}(\theta, \varphi, \chi)$, given by Eq. (3). Two Euler angles, θ and χ , were expressed as functions of a new set of Euler angles ($\theta_p, \varphi_p, \chi_p$) locating the (average) preferential axis of the polymeric chains, according to the following equations (derived by means of simple Euler angle rotational transformations in space (Puppulin et al., 2011):

$$\theta = \arccos(\cos \beta \cos \theta_p - \cos(\alpha + \varphi_p) \sin \beta \sin \theta_p) \quad (5)$$

$$\chi = \arcsin\left\{\frac{\cos \alpha \cos \chi_p \sin \beta \sin \varphi_p + \sin \chi_p (\cos \beta \sin \theta_p - \cos \theta_p \sin \alpha \sin \beta \sin \varphi_p) + \cos \varphi_p \sin \beta (\cos \chi_p \sin \alpha - \cos \alpha \cos \theta_p \sin \chi_p)}{\sqrt{1 - [\cos \beta \cos \theta_p - \cos(\alpha + \varphi_p) \sin \beta \sin \theta_p]^2}}\right\} \quad (6)$$

where the independent set of Euler angles (α, β, γ) describes the rotations in space of the Cartesian frame integer to the molecular orientation axes, $(x_{\text{mol}}, y_{\text{mol}}, z_{\text{mol}})$, within the polarized Raman probe, with respect to the axes of preferential orientation of the molecular structure, (x_p, y_p, z_p) (cf. Fig. 12(b)). The orientation distribution function, $f(\beta)$, was set as (Gurp, 1995; Liu and Kumar, 2003; Pérez et al., 2008):

$$f(\beta) = A \exp\{-[\lambda_2 P_2(\cos \beta) + \lambda_4 P_4(\cos \beta)]\} \quad (7)$$

where A is a constant and the parameters λ_2 and λ_4 are referred to as Lagrange multipliers (Jaynes, 1957). Note that in the computational procedure, we considered the Euler angle, φ , as a constant equal to φ_p , namely we neglected any torsional rotation of the molecular chains around their c -axis of the crystalline cell. In addition, we excluded, in first approximation, any azimuthal dependence of the orientation distribution function, which is thus taken only dependent on

one polar angle, β (i.e., thus assuming the existence of an uniaxial symmetry with respect to the preferential orientation of the molecular chains). Experimental Raman intensities collected upon in-plane rotation of the probe volume enable to set Eq. (4), in which we substituted for Eqs. (5)–(7), to find five unknown parameters: $\theta_p, \varphi_p, \chi_p, \lambda_2$, and λ_4 . The high number of variables involved in the integration and the large number of collected points in the polyethylene structure rendered the computation quite cumbersome (i.e., the full analysis required few weeks in our case). It should be noted, however, that we purposely collected in the interval, $0^\circ \leq \chi \leq 180^\circ$, $n=10$ relative intensity values at each investigated location, a number that largely exceeded the number of unknown parameters. From any five independent equations, we obtained the unknown parameters, $\theta_p, \varphi_p, \chi_p, \lambda_2$, and λ_4 , according to a best fitting procedure, while using the remaining equations for a confirmation of the obtained values. An additional computational routine was then needed for determining the two unknown parameters A and $\langle P_2(\cos \beta) \rangle$. Lagrange multipliers, λ_2 , and λ_4 , calculated by the aforementioned fitting procedure, enabled solving a system of two additional equations, as follows (Gurp, 1995; Liu and Kumar, 2003; Pérez et al., 2008):

$$\int_{\gamma=0}^{\gamma=2\pi} \int_{\alpha=0}^{\alpha=2\pi} \int_{\beta=0}^{\beta=2\pi} f(\alpha, \beta, \gamma) \sin \beta d\beta d\alpha d\gamma = 1 \quad (8)$$

$$\int_{\gamma=0}^{\gamma=2\pi} \int_{\alpha=0}^{\alpha=2\pi} \int_{\beta=0}^{\beta=2\pi} P_2(\cos \beta) f(\beta) \sin \beta d\beta d\alpha d\gamma = \langle P_2(\cos \beta) \rangle \quad (9)$$

In particular, by solving Eq. (9), the “order parameter”, $\langle P_2(\cos \beta) \rangle$, or Hermans orientation parameter, can be obtained. This parameter describes the statistical distribution of the molecular structure. Its value 0 indicates that the molecular orientation is fully random, while values 1 and -0.5 represent a perfect orientation parallel and perpendicular to the preferential orientation axis, respectively. In the conventions adopted in this study, the calculated value of θ_p represents the out-of plane tilt angle with respect to the uniaxially loaded surface of the polyethylene bearing. This angle, thus, gives a direct indication of the main microstructural modification expected to occur in a polymeric structure subjected to a compressive strain field applied along a direction perpendicular to the bearing surface.

4. Results and discussion

4.1. Crystallinity of as-received and plastically strained liners

As a first step in the presented structural characterizations, the evolution of amorphous and crystalline phase fractions contained within the microstructures of the three types of investigated UHMWPE liners have been monitored with respect to their response to compressive strain fields of increasing magnitude. The as-received materials were assumed to be in a residual strain-free state, while a static (uniaxial) strain magnitude was increasingly applied in order to reach, after unloading and successive strain recovery, two

sequential levels of plastic deformation at around 5 and 10% strain (i.e., henceforth simply referred to as residual strain after recovery, ε). Displacements in the order of $\approx 300\text{--}600\ \mu\text{m}$ obtained upon plastic deformation (i.e., $\approx 5\text{--}10\%$ residual strains in the 6-mm liner thickness) were achieved, which appear to be comparable with those expected to occur *in vivo*. Fig. 3 shows plots of amorphous phase fraction, α_a , (data for Liners A, B, and C in (a), (b), and (c), respectively) and crystalline phase fraction, α_c , (data for Liners A, B, and C in (d), (e), and (f), respectively) at three successive levels of residual strain, $\varepsilon = 0, \approx 5$, and $\approx 10\%$ after recovery. Data are plotted as a function of depth, z_{lab} , taken along the sub-surface from the pristine concave surface of the liner. The obtained $\alpha_a(z_{lab})$ and $\alpha_c(z_{lab})$ plots were markedly non-linear in all the investigated materials and experienced distinct variations of property gradients among each other. Their comparison clearly revealed the somewhat competitive effect of gamma-irradiation and vitamin E infusion on the final material microstructure. The main items obtained from Fig. 3 can be summarized as follows:

- (i) All the as-received liners experienced the lowest degree of crystallinity ($\approx 40\text{--}43\%$) on their concave surfaces. This common effect is interpreted as a consequence of surface machining, which was the same for all the investigated liners.
- (ii) The crystalline phase fraction rose up to about 50% (beyond a sub-surface depth of about $35\ \mu\text{m}$) and then saturated in Liner A, which reflects the characteristic structure of the resin GUR 1050 commonly selected as a starting material. On the other hand, the as-received Liner B and C, although prepared from the same starting resin as Liners A, reached

higher crystallinity values (in the order of about 52 and 55%, respectively) in their bulk ($z_{lab} \geq 50\ \mu\text{m}$). When comparing the processing procedures among the three investigated liners, as listed in Fig. 1, the crystallinity differences can be attributed to the effect of different gamma irradiation doses. Liner C exhibited the highest crystallinity values owing to the fact that it received the highest irradiation dose (totally 133 kGy) among the three types of liners. However, terminal (sterilizing) irradiation of 33 kGy for Liner C might have not contributed to crystallization and formation of crosslinking because of the obstructive effect (Oral et al., 2008) of infused vitamin E with respect to radiation crosslinking efficiency. Barron and Birkinshaw (2008) showed a crystallinity value of 53.7% for 100-kGy irradiated GUR 1050 by using Raman spectroscopy, which is a level of crystallinity comparable with our data for Liner C. This fact seems to suggest that there is no loss of crystallinity in Liner C either during vitamin E infusion or in the subsequent homogenization heating treatment below its melting point ($< 130\ ^\circ\text{C}$).

- (iii) Liner A, which received no irradiation dose, showed large increases in crystallinity (especially in its bulk) with increasing the magnitude of plastic strain. A small phase-structure variation was seen within the first $10\ \mu\text{m}$ below the surface upon increasing level of plastic strain. On the other hand, large fluctuations were observed in its bulk beyond a subsurface-depth of about $20\ \mu\text{m}$. However, the impact of plastic strain on the crystallinity of Liner A was insignificant within the investigated strain interval $\varepsilon \approx 5\text{--}10\%$.
- (iv) Liner B, which only received 33-kGy irradiation dose as a sterilization process, showed the largest fluctuations within the first $35\ \mu\text{m}$ below the surface among the three liners and significant increase in crystallinity upon increasing plastic

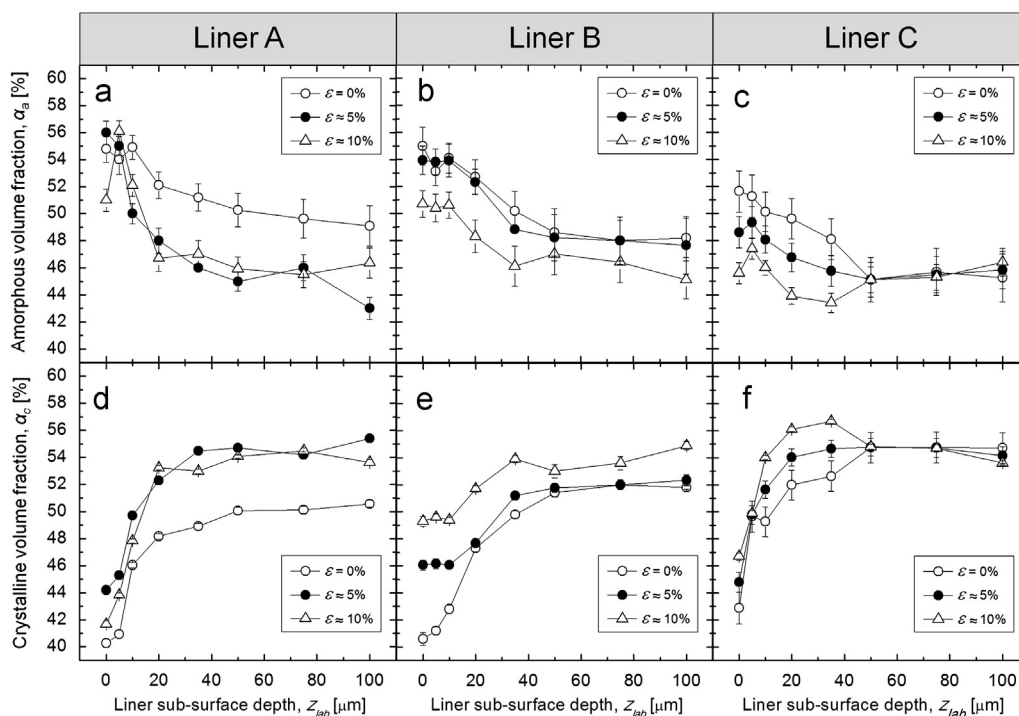


Fig. 3 – Depth profiles of phase volume fraction for Liners A, B, and C, as recorded upon different values of applied compressive strain ((a)–(c) amorphous fraction, α_a , and (d)–(f) for crystalline fraction, α_c).

strain. Below 50 μm in depth, small crystallinity variations were observed, meaning that strain did not significantly affect the bulk structure of the liner.

(v) The small crystallinity fluctuations ($(\Delta\alpha_c)_{\text{max}} \approx 4\%$) that were observed in Liner C were confined to a depth $< 35 \mu\text{m}$, while the bulk structure was almost constant

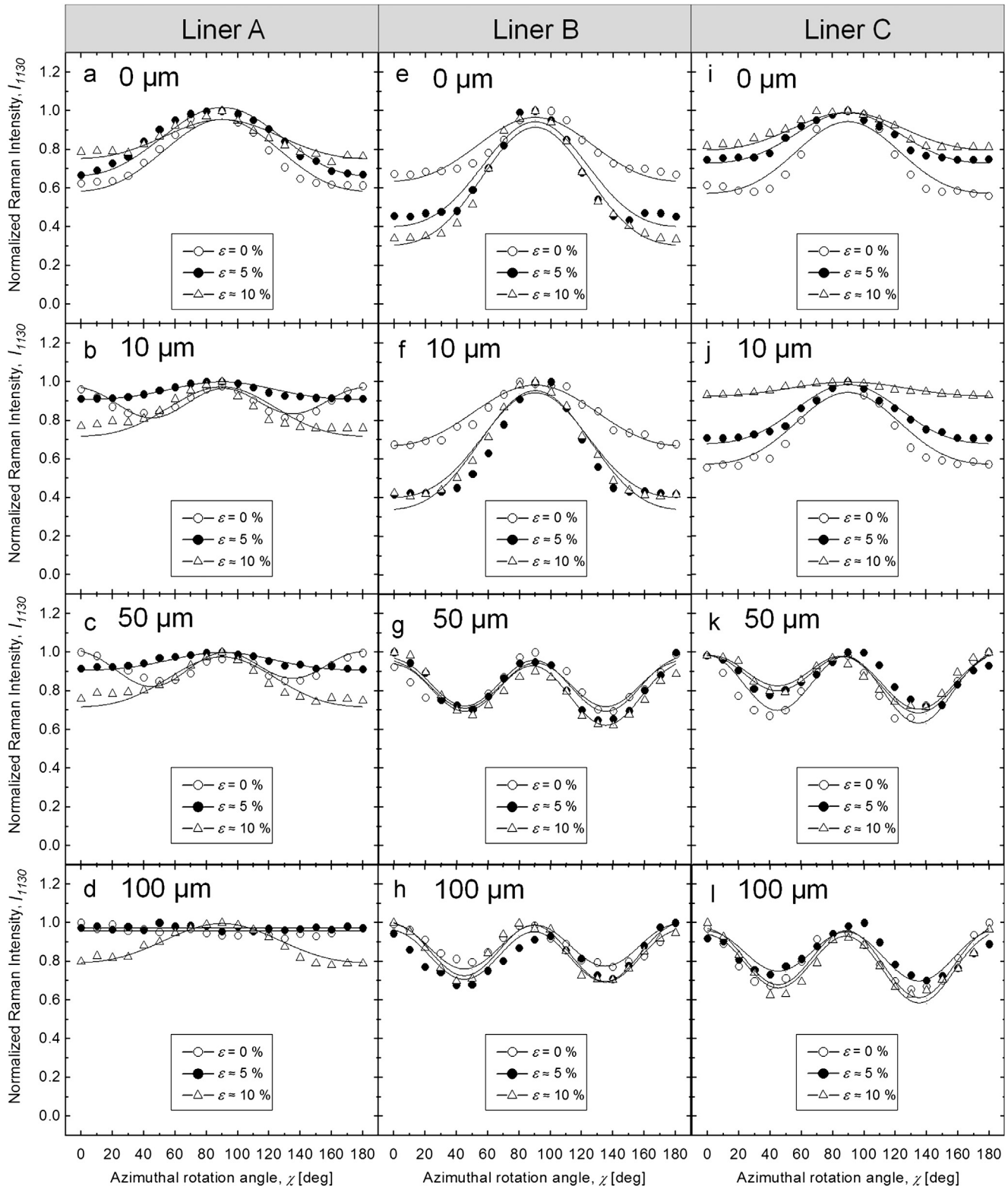


Fig. 4 – Experimental plots of angular dependence of the polarized Raman scattering intensities recorded upon in-plane rotation at different depth of Liner A-C ((a)–(d) for Liner A, (e)–(h) for Liner B, and (i)–(l) for Liner C). Full lines represent the results of best fitting to the experimental data according to Eqs. (4)–(9).

upon increasing strain magnitude. This observation suggests that, phenomenologically, the impact of plastic strain on the microstructure of Liner C was mitigated by the presence of crosslinking.

- (vi) Plots of amorphous (Fig. 3(a)–(c)) and crystalline (Fig. 3(d)–(f)) phase fractions, as detected either before or after plastic deformation, represented independent spectroscopic measurements and showed good consistency, the former plots decreasing while the latter increasing with increasing sampling depth. In all cases, the fractional amount of third (semi-crystalline) phase was found to be of a negligible entity.

4.2. Molecular orientation patterns in as-received and plastically strained liners

Fig. 4(a)–(d), (e)–(h), and (i)–(l) shows the experimental angular dependencies detected at different sub-surface depths by monitoring the behavior of the 1130 cm^{-1} band (A_g+B_{1g} Raman mode) on the azimuthal rotation angle, χ . The shown dependencies were obtained upon in-plane rotation at different stages of uniaxial deformation for the polyethylene structures of Liners A, B, and C, respectively. The key to interpret the azimuthal angular plots in Fig. 4 resides in considering the tendency to follow angular periodicities of π and $\pi/2$ for out-of-plane molecular alignments parallel ($\theta_p = 90^\circ$) and perpendicular ($\theta_p = 0^\circ$) to the liner surface, respectively. On the other hand, an increasing tendency toward a constant angular dependence of the Raman intensity on rotation angle indicates an increased degree of randomness in the molecular arrangement. With these notions in mind, the following considerations could be drawn from the plots in Fig. 4.

- (i) Liner A (Fig. 4(a)–(d)) presents a sharp (i.e., within the first $10\ \mu\text{m}$ below the surface) transition from a molecular alignment parallel to the sample surface to a nearly-random distribution, which is in fact the molecular pattern expected for a isostatically compression molded resin. The π periodicity is rather weak (i.e., with low

amplitude) also on the very surface of the sample and, similar to what we already observed for the crystallinity fraction in Fig. 3(d), the effect of uniaxial compressive strain does not appear to be very effective in altering the plot toward a higher amplitude. In other words, the molecular pattern did not show any strong tendency toward a higher degree of orientation parallel to the sample surface.

- (ii) Liners B and C (Fig. 4(e)–(h) and Fig. 4(i)–(l), respectively) showed very similar trends, with exactly the same $\pi/2$ periodicity and amplitude below a sub-surface depth of $50\ \mu\text{m}$. Above such depths, a compressive strain field in the range applied in this study appears to have almost no effect on the molecular alignment of both materials. However, the strain behaviors in the first $10\ \mu\text{m}$ of sub-surface depth were more complex and inherently different between the two materials. While in Liner B strain consistently enhanced the amplitude of the π -periodic dependence on azimuthal angle (thus pushing, as expected, a larger fraction of molecular chains to align their long-axis in a configuration parallel to the sample surface), in Liner C the applied compressive strain first pushed the surface molecular arrangement from π periodicity toward a random configuration (straight line), as an intermediate step to further achieve, beyond $10\ \mu\text{m}$, a $\pi/2$ periodicity.

A numerical procedure of least-square fitting to the collected experimental trends of (polarized) Raman intensities according to Eqs. (4)–(9) (cf. full lines in Fig. 4), enabled us to obtain plots of preferential (average) tilt angle, θ_p (Fig. 5), and Hermans parameter, $\langle P_2(\cos \beta) \rangle$ (Fig. 6), as a function of sample depth and for increasing level of plastic strain in the sample microstructures. Fig. 5(a)–(c) show tilt angle plots for Liners A, B, and C, respectively. A comparison among the three investigated materials better visualizes the strong similarity between the behaviors of Liners B and C, both materials undergoing sudden tilting rotation at the molecular scale along the sub-surface in order to develop textures perpendicular to the surface. When translated into terms of

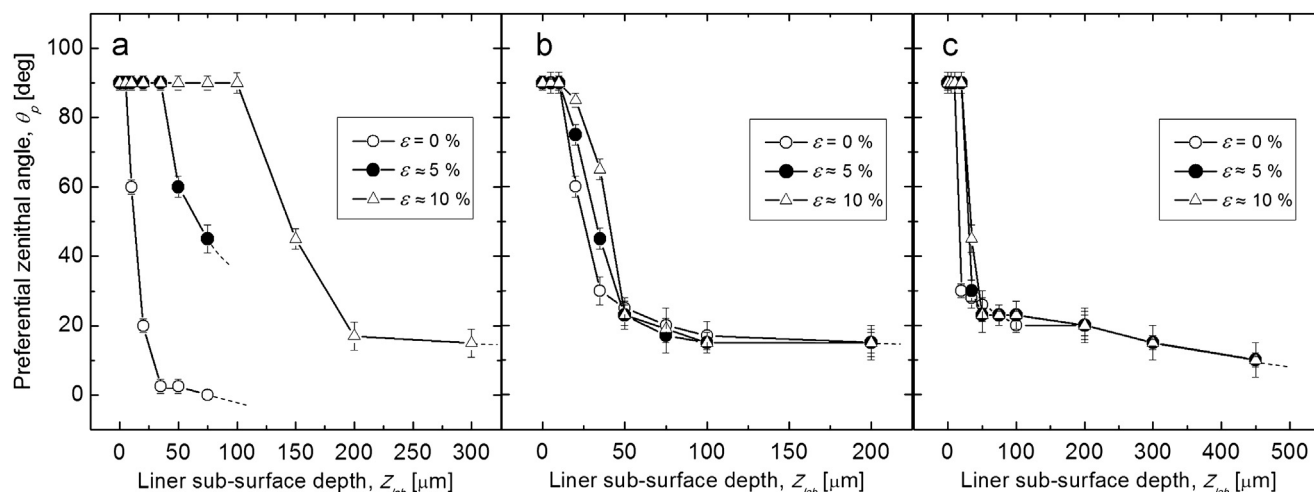


Fig. 5 – Depth profiles of average zenithal angle, θ_p , as calculated from the best fitting curves shown in Fig. 4 (data for Liners A, B, and C in (a), (b), and (c), respectively).

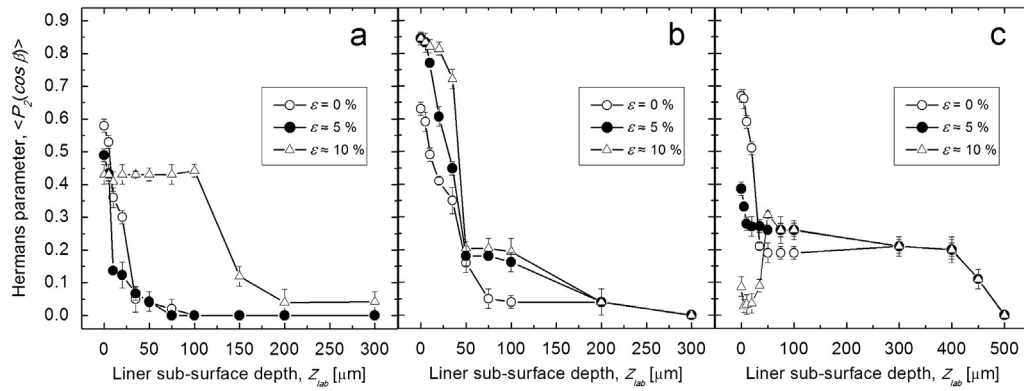


Fig. 6 – Depth profiles of Hermans parameter, $\langle P_2(\cos \beta) \rangle$, as calculated from the best fitting curves shown in Fig. 4 (data for Liners A, B, and C in (a), (b), and (c), respectively).

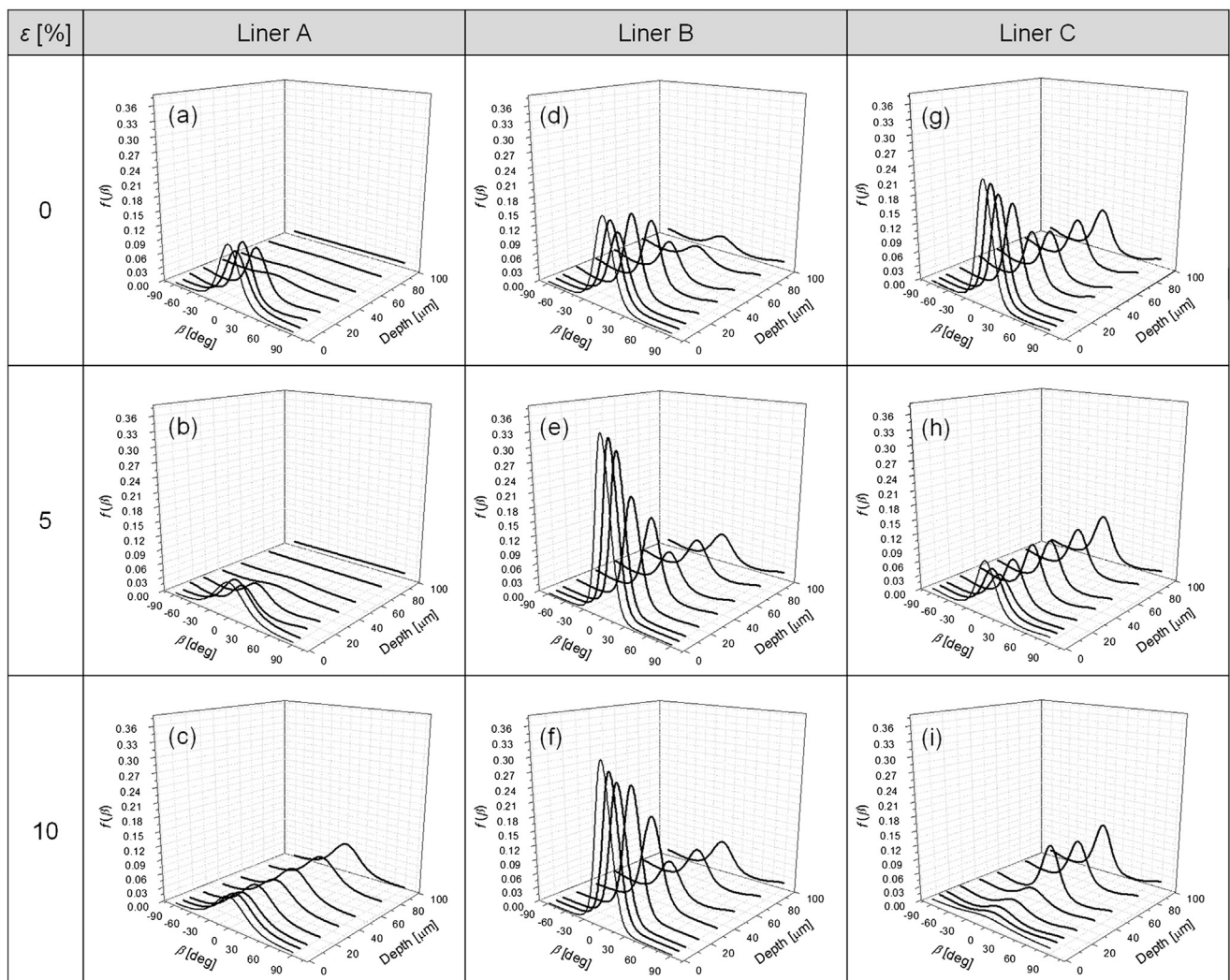


Fig. 7 – ODF at different depths in Liners A, B, and C, as retrieved after introducing different magnitudes of compressive strain in the microstructures ((a)–(c) for Liner A, (e) and (f) for Liner B, and (g)–(i) for Liner C).

tilting angles, the differences in periodicity induced by strain between Liners B and C (cf. Fig. 4) appear to fall into negligible differences in angular intervals. In the context of tilting angle variations, Liner A appears to possess by far the most pronounced dependence on strain among the investigated

liners, with showing a progressive textural alignment parallel to the sample surface with increasing the magnitude of compressive plastic strain stored in the material microstructure. It should be noted, however, that average angles are indeed representative of the texture but give no statistical

information about the actual molecular population that experiences the observed textured pattern in the polymer microstructure. The missing information can be obtained from plots of Hermans parameter (in Fig. 6(a)–(c) for Liners A, B, and C, respectively), as well as from drawing the full ODF distribution (Fig. 7) according to Eq. (7) as the function representative of the statistics of molecular tilt angles in the solid angle around the respective average values plotted in Fig. 5. The model Liner A (Fig. 6(a)), which lacked of cross-linked molecular chains, strikingly responded to strain on the molecular scale with a significant increase of the textured population parallel to the sample surface down to a depth of 100 μm . However, the overall ODF patterns for Liner A (cf. Fig. 7(a)–(c)), with or without incorporating plastic strain, always resulted much broader, and thus with textures much less relevant, than the other two liners under any strain condition. $\langle P_2(\cos \beta) \rangle$ plots in Fig. 6(b) and (c) revealed similar orientation homogeneity on the surface and in the immediate sub-surface of the as-received Liner B as compared to Liner C, although beyond 50 μm in depth Liner C appeared to retain a slightly higher degree of alignment. New physical insight, however, could be obtained when comparing the statistical evolutions of the molecular orientation patterns found in Liners B and C when they incorporated increasing amounts of plastic strain. While in the microstructure of Liner B the compressively strained molecular chains tended to gradually and consistently align parallel to the sample surface with increasing strain magnitude (cf. plots in Fig. 6(b) and the sharpening of the near-surface ODF distributions in Fig. 7(e) and (f) as compared to (d)), the opposite trend was observed for Liner C (Fig. 6(c)), in which plastic strain seems instead to have the effect of pushing the pre-existing texture toward more random patterns (i.e., $\langle P_2(\cos \beta) \rangle$ tending to zero). This effect was significant only within the first 50 μm below the sample surface, as can be easily visualized in the gradual smearing out over broader angular populations of the ODF distributions in Fig. 7(h) and (i) as compared to (g). The structural data collected in this and in the previous section represent the underlying foundation of the discussion given in the next section, which aims at interpreting the impact of different microstructural characteristics on the functionality of the liners.

4.3. Microstructural characteristics and the role of vitamin E in their development

According to the plots in Figs. 3, 5, and 7, we have phenomenologically clarified the salient structural differences induced by different processing steps involved with the respective manufacturing procedures of the studied liners. Moreover, clear differences came into view regarding the response of different microstructures to uniaxial compressive strain. However, in the two previous sections, a fundamental question was left unanswered which deals with the structural reason behind the different impact of plastic strain on both crystallinity and molecular chain orientation observed in different liners.

Liner C, even after infusion of vitamin E, seems to preserve acceptable crystallinity levels, achieved by the 100-kGy irradiation injected in the liner before vitamin E infusion. Any

obstructive effect of vitamin E (Oral et al., 2008), thus, could only have taken place during application of the final sterilization gamma-ray dose of 33 kGy. Oral et al. (2007) discussed in detail about the phenomenon of diffusion of vitamin E into irradiated UHMWPE. The crystalline phase of the polymer was considered to be conspicuously impermeable to large molecules like α -tocopherol, and the diffusion of vitamin E was assumed to primarily occur through the amorphous phase. Moreover, the presence of crystalline regions hindered (although with an effect conspicuously independent of irradiation dose) the diffusion of molecules by restricting diffusion pathways, which in turn produced a further decrease in magnitude of diffusion coefficient through the amorphous network of the semicrystalline polymer as compared to a bulk amorphous material. Given these physical circumstances, it follows that promoting appreciable diffusion of vitamin E through the bulk of a semicrystalline UHMWPE liner would require enhancing temperature with eventually applying external pressure. The most obvious procedure to overcome the difficulty encountered in diffusing the antioxidant phase through the UHMWPE bulk was proposed by Wolf et al. (2006). Those researchers introduced a homogenization step in inert atmosphere and super-critical carbon dioxide at temperatures above the melting point of cross-linked UHMWPE (> 135 $^{\circ}\text{C}$). However, such procedure is not viable in advanced liners because it would just lead to remelting the material, thus conspicuously invalidating any positive effect of the irradiation dose superimposed prior to homogenization. Oral et al. further inquired about the possibility of developing a homogenization method to penetrate vitamin E in highly crosslinked UHMWPE joint components without remelting the material (Oral et al., 2008; Oral and Muratoglu, 2011). Homogenization at 120 $^{\circ}\text{C}$ in inert gas, thus well below the melting point of the polymer, was found capable to diffuse vitamin E down to several millimeters below the surface of highly irradiated liners. The maker of the vitamin E-infused Liners C studied in this paper did not disclose the full details of the homogenization process, therefore we have no way to know whether the followed process was exactly the same as that described by these studies (Oral et al., 2008; Oral and Muratoglu, 2011). However, what we have experimentally observed in analyzing Liner C is that its crystallinity preserved a value comparable to the crystallinity level of 100-kGy irradiated GUR1050 UHMWPE (Barron and Birkinshaw, 2008), namely without any remelting effect of UHMWPE during homogenization heat treatment (cf. Fig. 3(f)). This fact can be considered as an evidence for no significant changes in microstructure (and presumably in mechanical properties) to occur during the homogenization procedures.

Regarding the effect of plastic strain on the material microstructure, the differences found in comparing Liners B and C were substantial. Data in Fig. 7 shows that the profile trends reached in Liner C at increasing levels of plastic strain were rather similar to those displayed by Liner A than to those recorded for Liner B. Liner C showed an increasing degree of randomness with increasing compressive strain (cf. Fig. 7(g)–(i)). This characteristic greatly contrasts with the significant sharpening of molecular chain distribution observed in Liner B under compressive strain (cf. Fig. 7(d)–(f)).

According to general notions from the field of deformation of bulk polymers (Bartczak et al., 1992; Lin and Argon, 1994), the response of semi-crystalline UHMWPE to strain should be considered to begin with a main deformation process occurring within amorphous regions, immediately followed by the activation of plastic slips inside the crystalline lamellae. In the initial stage of deformation, no significant rotation of crystalline lamellae should be found, with all the strain absorbed by microscopic displacements within the amorphous regions. After saturation of such displacements, crystalline lamellae

start zenithal rotations toward a configuration perpendicular to the applied compressive load. The ability of responding to compressive strain with a geometrical rotation is a measure of the overall chain mobility. Bartczak (2010) and Boontongkong et al. (1998) have shown that, in UHMWPE materials strained to a relatively low range of deformation, the microstructural texture experiences a higher degree of crystallographic orientation when it possesses a higher degree of crosslinking. This is because, in presence of a high degree of crosslinking, the molecular chains in the amorphous region

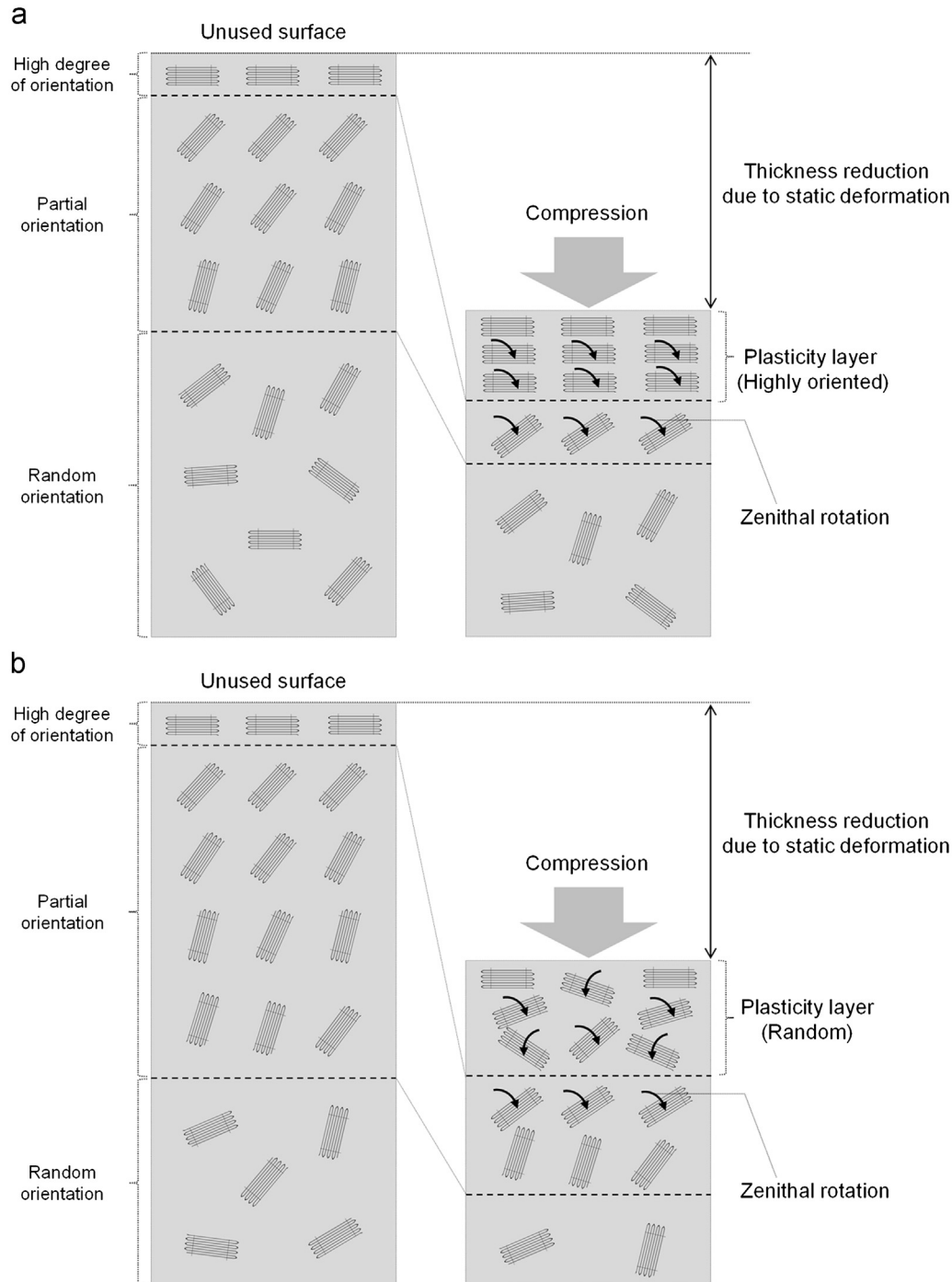


Fig. 8 – Schematics of molecular orientation pattern in liners obtained from isostatically compression molded UHMWPE resin. The deformation models in (a) and (b) refer to Liner B and C, respectively.

might quickly become fully stretched to their maximum limit. With amorphous regions incapable to incorporate additional displacements on the microscopic scale, strain is thus transmitted to crystalline lamellae that, under its effect, reorient perpendicular to the applied load. Our data for Liner A and B indeed agrees with the microstructural model proposed by Bartczak (2010) and Boontongkong et al. (1998), showing the most insensitive response to strain in the unirradiated (and therefore lacking of crosslinking) Liner A, and with Liner B, which possesses higher degree of crosslinking, showing higher microstructural mobility as compared to Liner A (cf. angular distribution trends in Fig. 7). However, Liner C, which presumably possesses the highest degree of crosslinking, did not follow the above mentioned model, and in fact, the microstructural response to strain (i.e. the increasing randomness observed upon strain application) of Liner C was closer to that of an unirradiated material than to that of an irradiated one. This behavior may indicate that the chain mobility of polyethylene became significantly lower by infusing α -tocopherol. The above notions are summarized in Fig. 8(a) and (b), which show drafts describing the deformation behavior under compressive load of Liners B and C, respectively.

In their seminal contribution on the effect of molecular orientation on the wear behavior of UHMWPE, Wang et al. (1997) showed that, in the multi-directional stress field experienced in hip joints, the UHMWPE bearing surface might undergo a strain-softening (weakening) effect related to structural anisotropy. Strain softening results in shear rupture and in the formation of fibrillar or filmy wear particles of UHMWPE. In order to minimize the detrimental effect that this phenomenon induces on wear behavior, a homogeneous and isotropic structure should be created at the surface of the liner and maintained during its functional activity. From this point of view, the increase in near-surface isotropy detected under compressive strain in Liner C might render the surface of this liner ideal to resist wear degradation (i.e., as suggested by the nearly tenfold reduction in *in-vitro* wear rate published by the maker in comparison to its previous product, Liner B (Biomet Biomaterials Laboratory, 2007)).

So far, very few studies have been published on the possible effect of vitamin E addition to UHMWPE, which is not affected by confounding factors related to irradiation and crosslinking. However, *in-vitro* knee simulator study performed by Teramura et al. (2008) proved that wear performance was consistently improved by just adding vitamin E into uncrosslinked polyethylene. The reason for such improvement remained unclear in that paper. Interestingly, our microstructural comparison upon static strain application between Liner B and C could help the interpretation of the wear behavior reported by Teramura et al. (2008), showing an increase in orientational randomness induced by the presence of vitamin E after plastic deformation. This phenomenon can reduce the amount of wear associated with strain softening.

Recent clinical study reported by Glyn-Jones et al. (2008) have shown the creep and wear behavior of conventional and highly crosslinked polyethylene liners over a short-term implantation time (i.e., 3 years) using radio-stereometric analysis. These researchers showed that penetration of the femoral head onto the liner was creep-dominated in the first six months of implantation; while, after one year, the creep

component of the overall migration displacement saturated and virtually all the additional penetration became due to wear. This indicates that a superior wear performance for Liner C can be expected also in *in vivo* use in comparison to Liner B, owing to the lowered risk of strain-softening. However, *in vivo* studies for Liner C are still underway, and a concern arises from the isotropically random molecular orientation possessed by its bulk structure. The occurrence of a marked reduction of creep resistance in isotropic polyethylene as compared to oriented polyethylene is a long known notation (Philip et al., 1986). From this point of view, the poor texture in Liner C induced by isostatically compression molding does not appear to have been designed to maximize creep resistance. The “molecular randomization” effect caused by plastic deformation in Liner C could be efficient in minimizing microscopic wear phenomena as mentioned above, but large deformations, which also lead to dimensional change in liner curvature and joint clearance, can trigger macroscopic wear enhancements due to a shape mismatch between femoral head and acetabular liner. Therefore, as long as we can judge from the present data, superior *in vivo* performance could be expected in Liner C only compared to the conventional product Liner B produced from the same isostatic polyethylene bar with poor texture. A final conclusion on whether the new material of Liner C could be more advanced compared to other highly-crosslinked UHMWPE materials currently available on the market is left to future studies.

5. Conclusion

The presented spectroscopic investigation builds upon the nowadays established chemical notion that vitamin E molecules potentially stabilizes free radicals throughout the structure of UHMWPE liners, allowing for vigorous gamma-irradiation without increasing the risk of oxidative degradation. We further inquire here about the consequences involved, on the microstructural and molecular scale, with the manufacturing choice of infusing an antioxidant substance in the UHMWPE structure. In particular, the two topics assessed in this paper deal with structural items related to the effect of vitamin E diffusion on crystallinity and molecular assembly. The studied UHMWPE structure was subjected to a robust (100 kGy) irradiation prior to vitamin E infusion and to a standard (33 kGy) sterilization/irradiation process after it. The obtained results can be summarized as follows:

- (i) With respect to the crystallinity ratio found on the sample surface and their profile along the sub-surface, vitamin E-infused liners showed no loss of crystallinity due to an homogenization process following the infusion of the antioxidant substance.
- (ii) In terms of microstructural texture, reflections of the orientation patterns induced by gamma-irradiation actually remained in the average tilt-angle profile along the sub-surface of the vitamin E-infused liner. However, the statistical distributions around such preferential orientation angles were completely annihilated by the effect of

compressive loading, which is beneficial to avoid strain-softening assisted wear phenomenon. This finding, revealed here for the first time by means of advanced Raman spectroscopic assessments, calls for a prompt and detailed confirmation of the static and dynamic deformation behaviors of this newly launched UHMWPE component.

The poor molecular textures observed in all the liners investigated in this study, which are the direct consequence of the choice of isostatically compression molded raw-material bars, could be detrimental to creep resistance *in vivo*, which could potentially lead to macroscopic wear enhancement due to a shape mismatch between femoral head and acetabular liner.

REFERENCES

- Amstutz, H.C., Campbell, P., Kossovsky, N., Clarke, I.C., 1992. Mechanism and clinical significance of wear debris-induced osteolysis. *Clinical Orthopaedics* 276, 7–18.
- Baker, D.A., Bellare, A., Pruitt, L., 2003. The effects of degree of crosslinking on the fatigue crack initiation and propagation resistance of orthopedic-grade polyethylene. *Journal of Biomedical Materials Research* 66A, 146–154.
- Barron, D., Birkinshaw, C., 2008. Ultra-high molecular weight polyethylene—evidence for a three-phase morphology. *Polymer* 49, 3111–3115.
- Bartczak, Z., 2010. Effect of chain entanglements on plastic deformation behavior of ultra-high molecular weight polyethylene. *Journal of Polymer Science Part B: Polymer Physics* 48, 276–285.
- Bartczak, Z., Argon, A.S., Cohen, R.E., 1992. Deformation mechanisms and plastic resistance in single-crystal-textured high-density polyethylene. *Macromolecules* 25, 5036–5053.
- Biomet Biomaterials Laboratory, 2007. E1TM antioxidant infused technology: the revolutionary second generation, vitamin E infused highly crosslinked UHMWPE. Available from URL: <http://www.biometeurope.fr/userfiles/files/Technologies/E1-Biomet-Lab-Paper.pdf> (accessed 28.05.12).
- Boontongkong, Y., Cohen, R.E., Spector, M., Bellare, A., 1998. Orientation of plane strain-compressed ultra-high-molecular-weight polyethylene. *Polymer* 39, 6391–6400.
- Bradford, L., Baker, D.A., Graham, J., Chawan, A., Ries, M.D., Pruitt, L.A., 2004. Wear and surface cracking in early retrieved highly cross-linked polyethylene acetabular liners. *Journal of Bone and Joint Surgery American* 86, 1271–1282.
- Bracco, P., Brunella, V., Zanetti, M., Luda, M.P., Costa, L., 2007. Stabilisation of ultra-high molecular weight polyethylene with vitamin E. *Polymer Degradation and Stability* 92, 2155–2162.
- Burton, G., Ingold, K., 1981. Autoxidation of biological molecules. 1. The antioxidant activity of vitamin E and related chain-breaking phenolic antioxidants *in vitro*. *Journal of the American Chemical Society* 103, 6472–6477.
- Collier, J.P., Currier, B.H., Kennedy, F.E., Currier, J.H., Timmins, G.S., Jackson, S.K., Brewer, R.L., 2003. Comparison of cross-linked polyethylene materials for orthopaedic applications. *Clinical Orthopaedics and Related Research* 414, 289–304.
- Currier, B.H., Currier, J.H., Mayor, M.B., Lyford, K.A., Collier, J.P., Van Citter, D.W., 2007. Evaluation of oxidation and fatigue damage of retrieved crossfire polyethylene acetabular cups. *Journal of Bone and Joint Surgery American* 89, 2023–2029.
- Digas, G., Kärrholm, J., Thanner, J., Malchau, H., Herberts, P., 2004. Highly cross-linked polyethylene in total hip arthroplasty. *Clinical Orthopaedics and Related Research* 429, 6–16.
- Gencur, S.J., Rinnac, C.M., Kurtz, S.M., 2003. Failure micro-mechanisms during uniaxial tensile fracture of conventional and highly crosslinked ultra-high molecular weight polyethylenes used in total joint replacements. *Biomaterials* 24, 3947–3954.
- Glotin, M., Mandelkern, L., 1982. A Raman spectroscopic study of the morphological structure of polyethylenes. *Colloid and Polymer Science* 260, 182–192.
- Glyn-Jones, S., McLardy-Smith, P., Gill, H.S., Murray, D.W., 2008. The creep and wear of highly cross-linked polyethylene: a three-year randomised, controlled trial using radiostereometric analysis. *Journal of Bone and Joint Surgery British* 90, 556–561.
- Gurp, M.V., 1995. The use of rotation matrices in the mathematical description of molecular orientations in polymers. *Colloid and Polymer Science* 273, 607–625.
- Harris, W.H., 1995. The problem is osteolysis. *Clinical Orthopaedics* 311, 46–53.
- Jaynes, E.T., 1957. Information theory and statistical mechanics. *Physical Review* 106, 620–630.
- Kamal-Eldin, A., Appelqvist, L., 1996. The chemistry and antioxidant properties of tocopherols and tocotrienols. *Lipids* 31, 671–701.
- Lerf, R., Zurbrugg, D., Delfosse, D., 2010. Use of vitamin E to protect cross-linked UHMWPE from oxidation. *Biomaterials* 31, 3643–3648.
- Lin, L., Argon, A.S., 1994. Review structure and plastic deformation of polyethylene. *Journal of Materials Science* 29, 294–323.
- Liu, T., Kumar, S., 2003. Quantitative characterization of SWNT orientation by polarized Raman spectroscopy. *Chemical Physics Letters* 378, 257–262.
- Muratoglu, O.K., Merrill, E.W., Bragdon, C.R., O'Connor, D., Hoeffel, D., Burroughs, B., Jasty, M., Harris, W.H., 2003. Effect of radiation, heat, and aging on *in-vitro* wear resistance of polyethylene. *Clinical Orthopaedics and Related Research* 417, 253–262.
- Naylor, C.C., Meier, R.J., Kip, B.J., Williams, K.P.J., Mason, S.M., Conroy, N., Gerrard, D.L., 1995. Raman spectroscopy employed for the determination of the intermediate phase in polyethylene. *Macromolecules* 28, 2969–2978.
- Oral, E., Godleski, Beckos., C., Malhi, A.S., Muratoglu, O.K., 2008. The effects of high dose irradiation on the cross-linking of vitamin E-blended ultrahigh molecular weight polyethylene. *Biomaterials* 29, 3557–3560.
- Oral, E., Muratoglu, O.K., 2007. Radiation cross-linking in ultra-high molecular weight polyethylene for orthopaedic applications. *Nuclear Instruments and Methods in Physics Research Section B: Beam Interactions with Materials and Atoms* 265, 18–22.
- Oral, E., Muratoglu, O.K., 2011. Vitamin E diffused, highly crosslinked UHMWPE: a review. *International Orthopaedics* 35, 215–223.
- Oral, E., Rowell, S.L., Muratoglu, O.K., 2006. The effect of α -tocopherol on the oxidation and free radical decay in irradiated UHMWPE. *Biomaterials* 27, 5580–5587.
- Oral, E., Wannomae, K.K., Rowell, S.L., Muratoglu, O.K., 2007. Diffusion of vitamin E in ultra-high molecular weight polyethylene. *Biomaterials* 28, 5225–5237.
- Pérez, R., Banda, S., Ounaies, Z., 2008. Determination of the orientation distribution function in aligned single wall nanotube polymer composites by polarized Raman spectroscopy. *Journal of Applied Physics* 103, 074302-1-9.
- Pezzotti, G., Kumakura, T., Yamada, K., Tateiwa, T., Puppulin, L., Zhu, W., Yamamoto, K., 2007. Confocal Raman spectroscopic analysis of cross-linked ultra-high molecular weight polyethylene for application in artificial hip joints. *Journal of Biomedical Optics* 12, 014011 011.
- Philip, M., Ward, I.M., Parsons, B., 1986. A comparison of tensile, compressive and torsional creep in isotropic and oriented polyethylene. *Journal of Materials Science* 21, 879–886.
- Puppulin, L., Takahashi, Y., Zhu, W., Sugano, N., Pezzotti, G., 2011. Polarized Raman analysis of the molecular rearrangement

- and residual strain on the surface of retrieved polyethylene tibial plates. *Acta Biomaterialia* 7, 1150–1159.
- Rull, F., Prieto, A.C., Casado, J.M., Sobron, F., Edwards, H.G.M., 1993. Estimation of crystallinity in polyethylene by Raman spectroscopy. *Journal of Raman Spectroscopy* 24, 545–550.
- Strobl, G.R., Hagedorn, W., 1978. Raman spectroscopic method for determining the crystallinity of polyethylene. *Journal of Polymer Science Part B: Polymer Physics* 16, 1181–1193.
- Takahashi, Y., Puppulin, L., Zhu, W., Pezzotti, G., 2010. Raman tensor analysis of ultra-high molecular weight polyethylene and its application to study retrieved hip joint components. *Acta Biomaterialia* 6, 3583–3594.
- Teramura, S., Sakoda, H., Terao, T., Endo, M.M., Fujiwara, K., Tomita, N., 2008. Reduction of wear volume from ultra-high molecular weight polyethylene knee components by the addition of vitamin E. *Journal of Orthopaedic Research* 26, 460–464.
- Wang, A., Sun, D.C., Yau, S.-S., Edwards, B., Sokol, M., Essner, A., Polineni, V.K., Stark, C., Dumbleton, J.H., 1997. Orientation softening in the deformation and wear of ultra-high molecular weight polyethylene. *Wear* 203–204, 230–241.
- Wang, A., Zeng, H., Yau, S.-S., Essner, A., Manely, M., Dumbleton, J., 2006. Wear, oxidation and mechanical properties of a sequentially irradiated and annealed UHMWPE in total joint replacement. *Journal of Physics D: Applied Physics* 39, 3213–3219.
- Wannomae, K., Bhattacharyya, S., Freiberg, A., Estok, D., Harris, W.H., Muratoglu, O., 2006. *In vivo* oxidation of retrieved cross-linked ultra-high-molecular-weight polyethylene acetabular components with residual free radicals. *Journal of Arthroplasty* 21, 1005–1011.
- Wolf, C., Maninger, J., Lederer, K., Fruhwirth-Smounig, H., Gamse, T., Marr, R., 2006. Stabilisation of crosslinked ultra-high molecular weight polyethylene (UHMW-PE)-acetabular components with alpha-tocopherol. *Journal of Materials Science Materials in Medicine* 17, 1323–1331.